A MONTE CARLO STUDY OF THE MESOPHASES FORMED BY POLAR BENT–SHAPED MOLECULES

Silvia Orlandi, Roberto Berardi, Joachim Steltzer and Claudio Zannoni,

Dipartimento di Chimica Fisica e Inorganica and INSTM.
Università di Bologna.
Viale Risorgimento 4, 40136 Bologna, Italy.

December 14, 2005

Abstract

Liquid crystal phases formed by bent shaped (or "banana") molecules are currently of great interest. Here we investigate the phases formed by banana molecules modelled combining three Gay–Berne sites and containing either one central or two lateral and transversal dipoles. We show that changing the dipole position has a profound effect on the mesophase stability and molecular organisation. In particular we find a nematic phase only for off centre dipoles and tilted phases only for terminal dipoles.

1 Introduction

Liquid crystals formed by banana-shaped molecules have provoked a great interest since their discovery and the demonstration of electro-optic switching in some of the tilted phases they form.[1–3] Novel materials of this type continue to appear and their properties to be unveiled. For instance, Samulski et al. have recently proposed, on the basis of X-rays spectroscopy[4] and NMR[5] evidence, the formation of biaxial nematic phases from bow shaped molecules.

Part of the excitation created by the discovery of banana phases was caused by the formation of chiral phases like the so called B_2 phase resulting from non-chiral polar molecules and the attendant ferroelectric behaviour.[3,6] The proposed mechanism[6,7] relies on the formation of tilted smectic phases, where the layers become chiral because of the removal of reflection symmetry caused by the combination of the tilt itself and the presence of transversal layer polarity.[8]

On the other hand it has been pointed out by Takezoe et al. that, due to the conformational freedom of the mesogens, the existence of a more straightforward mechanism based on chiral conformations is also possible[9] and indeed twisted conformers have recently been detected by ^{13}C NMR in banana phases.[10] Moreover some of the banana mesogens have been found to behave as a chiral dopant when added to a cholesteric,[9] or to exhibit spontaneous twist.[2,11]

It is thus particularly important to identify some of the basic features that a molecule should possess to be a good candidate for exhibiting a supermolecular chiral phase.[12] In particular, what phases can we get starting from a truly non chiral, polar and rigid bent mesogen? From the modelling and computer simulation point of view this requires going beyond the simple symmetric models such as the standard Gay-Berne (GB) one with ellipsoidal shape[13] and build a minimal banana shaped mesogen.

Some simulations have appeared where banana molecules have been modelled join-

ing two hard spherocylinders[14–16] or with a bent arrangement of spheres.[17,18] Other models are based on two GB particles connected at an end with a chosen angle either rigidly[19–21] or through a spring.[22] These simulations differ in the details of the GB parametrization, and give evidence that bent molecules can form the nematic phase above a critical bending angle (which is the angle between the wings of the bent molecule). The amplitude of the inter-arm angle has also been pointed out as important for the formation of a biaxial nematic phase.[23] The formation of spontaneously twisted structures in nematic phases, albeit surprising, has been reported in the computer simulations of model achiral banana particles by Memmer.[21]

One feature invariably present in real banana mesogens but, as far we know, missing from current modelling, is the presence of one or more permanent dipoles. It is clear that the position of the dipoles can affect the phase stability[24] and the possibility of getting tilted phases,[25] Indeed, when a permanent dipole has been added to rod shaped GB mesogens, important modifications have been observed for the molecular resulting organization.[26,27] The effect of a dipole on mesophase stability depends on its position, orientation and strength, so that a detailed analysis is normally required.

The situation can be expected to be even more complex for bent particles, where the importance of the dipole contribution should be strongly coupled with form factor and interdigitation. Apart form these complications the presence of a dipole is crucial to the formation of phase chirality as currently understood.[3,6,8] We thus believe that dipoles should be included in a "minimal" banana model.

Here, we have explored the combined effects of shape and interaction polarity by simulating model systems formed by bent molecules (Fig. 1) with one or two point dipoles at different positions. As the model particles are rigid and strictly non chiral, the conformational mechanism for the formation of chiral phases is ruled out. In the following sections we describe the model employed and the simulations performed and we then concentrate on the results, particularly exploring

the formation of tilted smectic as well as the presence or not of biaxiality and of chiral superstructures.

2 Model and simulation

We consider a system of banana shaped molecules built from three equivalent ellipsoidal sub–units with axes $\sigma_x = \sigma_y$ and σ_z, where each of the uniaxial sites on a particle interacts with those on other molecules via a GB repulsive and attractive site–site potential. The potential between a pair of three-site molecules i and j is written as

$$U_{ij}^{GB}(\omega_i, \omega_j, \mathbf{r}_{ij}) = \sum_{a \in i, b \in j} U_{ab}^{GB}(\omega_a, \omega_b, \mathbf{r}_{ab}) \tag{1}$$

where the sum runs on distinct site–site interactions U_{ab}^{GB},

$$U_{ab}^{GB} = 4\epsilon(\omega_a, \omega_b, \hat{\mathbf{r}}_{ab}) \left[\left\{ \frac{\sigma_s}{r_{ab} - \sigma(\omega_a, \omega_b, \hat{\mathbf{r}}_{ab}) + \sigma_s} \right\}^{12} - \left\{ \frac{\sigma_s}{r_{ab} - \sigma(\omega_a, \omega_b, \hat{\mathbf{r}}_{ab}) + \sigma_s} \right\}^{6} \right] \tag{2}$$

and ω_a, ω_b are the orientations of the sites axes ($\mathbf{x}_a$,$\mathbf{y}_a$,$\mathbf{z}_a$), ($\mathbf{x}_b$,$\mathbf{y}_b$,$\mathbf{z}_b$) with reference to the laboratory frame of sites a, b, $\mathbf{r}_{ab} = r_{ab}\hat{\mathbf{r}}_{ab} = \mathbf{r}_b - \mathbf{r}_a$ are the intersite vectors. The contact distances $\sigma(\omega_a, \omega_b, \hat{\mathbf{r}}_{ab})$ are characterized by the length to breadth ratio $\chi = \sigma_z/\sigma_x$, where $\sigma_x = 0.6\sigma_0$, the attractive terms $\epsilon(\omega_a, \omega_b, \hat{\mathbf{r}}_{ab})$ by the potential well depth ratio $\chi' = \epsilon_z/\epsilon_x$, where $\epsilon_x = 1\epsilon_0$, and two further parameters μ, ν.[13,28] Here we choose for the three sites $\chi = 8/3$, $\chi' = 5$, $\mu = 1$ and $\nu = 3$. The molecular model is characterized by two internal coordinates: the lateral sites positions, referred to the center of mass, and the bending angle ϕ between their lateral sites axes. For this study a bending angle of $\phi = 120°$ was chosen, a typical value in the range of banana–shaped molecules with a central phenyl unit. Sites centres positions, $(-0.122\sigma_0, 0, 0)$ for the central site, and $(0.061\sigma_0, 0, \pm 0.697\sigma_0)$ for the lateral ones, have been selected in order to have a considerable overlap of

the three GB sites and form a bent shape without large surface discontinuities. A schematic representation of the model, with the point dipoles also shown, is given in Fig. 1.

The dipolar energy is a sum of contributions given by the classic electrostatic expression:

$$U_{ij}^{d} = \sum_{a\in i, b\in j} \frac{1}{r_{ab}^{3}} \left[\boldsymbol{\mu}_a \cdot \boldsymbol{\mu}_b - 3(\boldsymbol{\mu}_a \cdot \hat{\mathbf{r}}_{ab})(\boldsymbol{\mu}_b \cdot \hat{\mathbf{r}}_{ab})\right] \tag{3}$$

where r_{ab} is the vector joining the point dipoles $\boldsymbol{\mu}_a$ and $\boldsymbol{\mu}_b$ on the molecules i, j. Here, and in the rest of the paper, we give all the lengths in units σ_0 and the energies in units ϵ_0, while the dimensionless dipole strength is $\mu^* \equiv (\mu^2/\epsilon_0\sigma_0^3)^{1/2} = 1$. The electrostatic energy has been evaluated using the reaction field method[29] with separation radius $r_{RF}^* = 4$, and with a dielectric continuum of permittivity $\epsilon_{RF} = 1.5$. Although this method is less rigorous than the Ewald summation, it has previously proved to be adequate for similar systems and sample sizes[30–32] and it allows great computational advantages.

We have studied here systems of $N = 1000$ rigid banana-shaped molecules performing temperature scans by Monte Carlo simulations in the isobaric–isothermal NPT ensemble at the reduced pressure $P^* \equiv P\sigma_0^3/\epsilon_0 = 10$. Periodic boundary conditions (PBC) and nearest image summation were applied. The MC cooling runs were started from well equilibrated isotropic configurations of dipole–less particles in a cubic box. After switching on the dipolar interactions, the simulations were run in a cooling sequence with equilibration runs of ≈ 300 kcycles, where a cycle corresponds to N attempted MC moves.

To minimize the formation of PBC artifacts or defects in the smectic phases, particularly the possibility of metastable states with anomalous tilt or interdigitation due to a mismatch betweeen the box size and layered structure equilibrium spacings, we have also allowed shape changes of the MC sample box to take place and performed simulations with a "variable" metric tensor.[33] This additional precaution (put forward by Yashonat and Rao in[33]) has been used with NPT ensemble

simulations only in few recent studies,[18,34] but it is clearly important here since we are interested in the possibility of tilted phases whose formation might be prevented by an orthogonal simulation box of finite size. If **a**, **b**, **c** are the principal axes of the simulation box, i.e. the not mutually orthogonal vectors defining the orientation of the faces and, in general, the different lenghts of the sides, then the so–called scaling matrix $\mathcal{H} = [\mathbf{a}, \mathbf{b}, \mathbf{c}]$, whose columns are the box axes, describes the volume $V = |\det \mathcal{H}|$, and the shape of the MC box.

The scaling matrix $\mathcal{H}$ defines the metric tensor as $\mathcal{G} = \mathcal{H}^T\mathcal{H}$,[35] and transforms the particles coordinates from real σ_0 units, r_α, to the scaled coordinates, s_α, according to $r_\alpha = \mathcal{H}s_\alpha$, where the scaled coordinates $s_\alpha = (s_x, s_y, s_z)$ give the particles positions in a cubic box with sides of unit length, while the real particles coordinates $r_\alpha = (r_x, r_y, r_z)$ describe the positions of the particles in a box whose size and shape are given by $\mathcal{H}$.

One MC cycle consists of a sequence of random attempts to update all the particle positions and orientations, using for the latter the standard Barker Watts algorithm.[29] The sampling of the scaling matrix $\mathcal{H}$ has been performed by random displacements of every element H_{ij}, generated, with a frequency of 10% with respect of the total number of attempted moves, according to $H^{new} = H^{old} + \Delta h_{max}(\epsilon - 1/2)$, where Δh_{max} is the maximum allowed displacement of an element, and ϵ is a 3×3 random matrix whose elements have been sampled from an uniform distribution ($0 \leq \epsilon_{ij} \leq 1$). Since all our samples are fluid and the standard NPT evolution algorithm[36] enforces only the diagonal elements of the stress tensor to be equal to the hydrostatic pressure, but does not impose constraints on the off-diagonal elements, we have put bounds on the box sides values so that the angles between the MC sample axes can not be lower than 60°, and $\det \mathcal{H} > 0$, so as to prevent the MC sample from assuming an extremely distorted shape.

In order to characterize the nature of the different phases of the systems studied we have determined various orientational order parameters computed from the

eigenvalues of the three ordering matrices relative to the $\mathbf{x}_i$, $\mathbf{y}_i$ and $\mathbf{z}_i$ molecular axes.[12,37] In particular the standard orientational order parameter

$$\langle P_2 \rangle = \left\langle \frac{3}{2}(\mathbf{z}_i \cdot \mathbf{Z})^2 - \frac{1}{2} \right\rangle \tag{4}$$

gives a measure of the average static alignment of the longest molecular axis, while phase biaxiality is instead monitored considering:

$$\langle R^2_{2,2} \rangle = \left\langle \frac{1}{4} \left[(\mathbf{x}_i \cdot \mathbf{X})^2 - (\mathbf{x}_i \cdot \mathbf{Y})^2 - (\mathbf{y}_i \cdot \mathbf{X})^2 + (\mathbf{y}_i \cdot \mathbf{Y})^2 \right] \right\rangle \tag{5}$$

which measures to what extent there is a difference in the ordering of the $\mathbf{x}$ and $\mathbf{y}$ molecular axis in the plane orthogonal to the system director, $\mathbf{Z}$. Moreover, in order to investigate the "polar", transversal, ordering we have calculated the first rank order parameter $\langle P^x_1 \rangle = \langle \mathbf{x}_i \cdot \mathbf{X} \rangle$ which quantifies the degree of alignment degree of the molecular transverse $\mathbf{x}$ axis with respect to the $\mathbf{X}$ direction of the director frame.

Structural assignments require a knowledge not only of the order of a molecule with respect to the laboratory frame, but also of the arrangement of one molecule with respect to another. This information was obtained via various pair distribution functions computed as discrete histograms from the simulated configuration. Particularly useful in smectic phases is the density along the director

$$g(z) = \frac{1}{\pi R^2 \rho} \langle \delta(z - z_{ij}) \rangle_{ij} \tag{6}$$

where $z_{ij} = \mathbf{r}_{ij} \cdot \mathbf{Z}$, is computed with respect to the director frame and R is the radius of a cylindrical sampling region. To determine if a phase is of the Smectic C type, we have also calculated the average tilt angle $\langle \alpha \rangle$, which is the angle between the phase director $\mathbf{Z}$ and the normal $\mathbf{n}$ to the smectic layers, computed with the procedure reported in detail in.[25]

We have calculated various average Stone rotational invariants,[38,39] as a function of intermolecular separation r. We report in particular two of them. The first,

useful in assessing biaxiality and its correlation length, is

$$S_{22}^{220}(r) = \frac{1}{4\sqrt{5}} \langle \delta(r - r_{ij}) \, (\, (\mathbf{x}_i \cdot \mathbf{x}_j)^2 - \, (\mathbf{x}_i \cdot \mathbf{y}_j)^2 - \, (\mathbf{y}_i \cdot \mathbf{x}_j)^2 + \, (\mathbf{y}_i \cdot \mathbf{y}_j)^2$$
$$-2 \, (\mathbf{x}_i \cdot \mathbf{y}_j) \, (\mathbf{y}_i \cdot \mathbf{x}_j) - 2 \, (\mathbf{x}_i \cdot \mathbf{x}_j) \, (\mathbf{y}_i \cdot \mathbf{y}_j)$$
$$+i(-2 \, (\mathbf{x}_i \cdot \mathbf{x}_j) \, (\mathbf{x}_i \cdot \mathbf{y}_j) - 2 \, (\mathbf{x}_i \cdot \mathbf{x}_j) \, (\mathbf{y}_i \cdot \mathbf{x}_j)$$
$$+2 \, (\mathbf{x}_i \cdot \mathbf{y}_j) \, (\mathbf{y}_i \cdot \mathbf{y}_j) + 2 \, (\mathbf{y}_i \cdot \mathbf{x}_j) \, (\mathbf{y}_i \cdot \mathbf{y}_j)))\rangle_{ij}. \tag{7}$$

measuring for a pair of particles at distance r the average orientational correlation between $\mathbf{x}_i$, $\mathbf{x}_j$, $\mathbf{y}_i$, $\mathbf{y}_j$ molecular axes. The second histogram, helpful in looking for twisted structures, is

$$S_{00}^{221}(r) = -\frac{\sqrt{3}}{\sqrt{10}} \langle \delta(r - r_{ij}) \, (\, (\mathbf{z}_i \cdot \mathbf{z}_j) \, (\mathbf{z}_i \cdot \mathbf{z}_j \times \hat{\mathbf{r}}_{ij}))\rangle_{ij}$$

that measures the average chiral correlation between the molecular $\mathbf{z}_i$ and $\mathbf{z}_j$ axes as a function of the distance r.[21,40]

As a further information on the polar correlations between molecular axes we have computed the average scalar product between the transverse axis $\mathbf{x}_i$ of a molecule i chosen as the origin and that of any molecule j found at a distance r, i.e. $\langle \delta(r - r_{ij}) \mathbf{x}_i \cdot \mathbf{x}_j \rangle_{ij}$, that in turn can be expressed as a linear combination of two first rank rotational invariants:

$$\langle \delta(r - r_{ij}) (\mathbf{x}_i \cdot \mathbf{x}_j) \rangle_{ij} = -\sqrt{3} \, \mathrm{Re}[S_{1,1}^{1,1,0}(r) - S_{1,-1}^{1,1,0}(r)]. \tag{8}$$

Finally, we have also calculated, whenever necessary for the characterization of the smectic phases obtained, the global hexatic order parameter $\langle \psi_6 \rangle$, average in the configurational space, of the parameter ψ_6 for each smectic layer $\mathcal{L}$ of a MC configuration[25,41]

$$\psi_6 = \frac{1}{N_{\mathcal{L}}} \sum_{m=1}^{N_{\mathcal{L}}} \frac{1}{N_m} \sum_{n=1}^{N_m} e^{i6\theta_{mn}}, \tag{9}$$

with $N_{\mathcal{L}}$ the number of molecules in the layer $\mathcal{L}$, N_m nearest neighbors of molecule m, and θ_{mn} the angle between position vector $\mathbf{r}_{mn}$ and an arbitrary fixed axis passing through m.

3 Results and discussion

Detailed results are presented here for a series of three–site polar banana-shaped GB models which differ for the dipoles number and position in the molecular frame (see Fig. 1). A preliminary set of runs was also performed for the dipole-less system in order to roughly locate the transitions and to obtain seeding configuration for the present simulations. The results for the order parameter of these runs are reported in Fig. 2. Starting from an isotropic phase every new run at a lower T^* began from the previously equilibrated temperature. All samples were cooled down using temperature steps of $\Delta T^* = 0.1$. The sequence of runs was stopped once the system had reached a nearly solid state.

3.1 One central dipole

We start discussing the system with one central dipole and we first notice (Fig. 2) that at $T^* = 4.0$ it shows a sharp phase transition directly from isotropic to smectic. This can be seen from the steep increase in the orientational order parameter which jumps from $\langle P_2 \rangle \approx 0.1$ to ≈ 0.9. The molecular organization as obtained from an equilibrium configuration of this smectic temperature just below the transition ($T^* = 3.8$) is shown in Fig. 3. The orientation of the molecules, with respect to the director, is rendered using a colour coding ranging from yellow (parallel) to blue (perpendicular). The view axis is along the laboratory **Y** direction and the director is aligned with the laboratory **Z** axis. The smectic phase obtained is strongly biaxial ($\langle R^2_{22} \rangle = 0.38$) and presents an hexagonal order within the layers (global hexatic order parameter $\langle \psi_6 \rangle = 0.68$). The longitudinal pair distribution function displays an oscillation indicating the presence of a layered system, while the examination of the radial pair distribution function $g(r)$ shows a splitting in the second group of peaks between $r^* = 1.2$ and $r^* = 1.4$ indicating, again, an hexagonal packing which identifies this as a smectic B phase, in agreement with

the large value of $\langle\psi_6\rangle$. Fig. 4 shows an exploded view of the four smectic layers of the same configuration, and we have used a polar colour map ranging from red to cyano to highlight the antiferroelectric ordering of the transverse molecular $\mathbf{x}$ axis with respect to the laboratory $\mathbf{X}$ axis (red for $\mathbf{x}$ parallel to $\mathbf{X}$, and cyano for $\mathbf{x}$ antiparallel to $\mathbf{X}$). From this snapshot a local polar arrangement of the dipoles with an alternating polarization direction between adjacent layers is immediately recognizable: all dipoles within the same smectic layer have a common transversal orientation, so that each layer has a net non zero polarization, but this is compensated in a antiferroelectric way by adiacent layers.

To characterize odd or even structures, the layers of the configurations produced by the MC evolution (and stored to compute the averages, see Table 1), were analyzed separately to obtain the in-plane polar order parameter $\langle P_1^x\rangle_{\mathcal{L}} = \langle \mathbf{x}_i \cdot \mathbf{X}\rangle_{\mathcal{L}}$, where the subscript $\mathcal{L}$ reminds that this quantity has been calculated separately for each smectic layer. We see (also from Table 1) that although there is no overall polarization, $|\langle P_1^x\rangle_{\mathcal{L}}| \approx 0.9$ inside each layer. The polar pair correlation has an average overall persistence of just one molecular lenght ($\approx 3\sigma_0$) as shown by $\langle\delta(r-r_{ij})(\mathbf{x}_i\cdot\mathbf{x}_j)\rangle_{ij}$ (Fig. 4, right), then decays to zero. This behaviour is different from that of the second rank correlation $S_{22}^{220}(r)$ which levels instead to ≈ 0.16. Since these two histograms were computed with a spherical sampling (and not considering only molecular pairs belonging to the same layer), when analysing the first rank invariant for distances larger than one molecular lenght, contributions of opposite sign arising from different layers annihilate, while this is not true for $S_{22}^{220}(r)$, confirming the conclusions drawn examining the exploded views of Fig. 4.

3.2 Two lateral dipoles

Turning now to the second model bent mesogen, we notice that two dipoles positioned at the centres of lateral GB sites (Fig. 1) induce a softening of the disorder–order transition and the appearance of a nematic phase (see Fig. 2), even if this is

stable only within a narrow temperature range. This phase has not been observed in the previous central dipole case, as well as in the corresponding dipole-less GB bent mesogen model. This behaviour is also accompanied by a shift of the order-disorder transition towards lower temperatures; this seems to indicate that the smectic phase is disfavoured by these dipolar interactions. However, at low temperature, a smectic A and a smectic B biaxial phase with high hexatic order (see also Table 1) was found. Examining a typical snapshot in the smectic B range ($T^* = 2.8$, see Fig. 5) no tilt of molecules is apparent. Instead, the structure is weakly interdigitated as showed also by the density along the director $g(z)$ (Fig. 5) which exhibits peaks broad and not very intense, suggesting that the dipolar interaction enhances the extent of interdigitation between layers. The smectic phase is biaxial as shown by the high value of order parameter $\langle R^2_{22} \rangle = 0.36$ and by the long–range behaviour of S^{220}_{22} (Fig. 6).

Again, a polar arrangement of in–layer dipoles is evident from an exploded view of the snapshot of the layers and from the polar pair correlation in Fig. 6.

3.3 Two terminal dipoles

Our third system has the two dipoles further shifted away from the centre (Fig. 1). The MC simulations show a different behaviour in the temperature dependence of $\langle P_2 \rangle$ (Fig. 2) with respect to the previous cases: the system still exhibits two ordering transitions (I-N and N-Sm), but here the one to a smectic phase is significantly moved towards lower temperatures. This leads to a wider nematic range, and a smectic phase which is characterized by high values of $\langle P_2 \rangle$ and a reduced biaxiality ($\langle R^2_{22} \rangle < 0.16$).

The snapshot of an equilibrium configuration of this system at $T^* = 3.2$, shown in Fig. 8, evidentiates that the smectic phase is now a tilted one, with an averaged tilt angle calculated as $\langle \alpha \rangle = 18°$. The direction of tilt is the same between adjacent layers, indicating that the phase is synclinic. In the current classification

of smectic a variety of phases exists, according to the presence of positional order and the details of tilt direction in the layers.[42] In particular smectic C corresponds to the absence of positional order. Here instead, each layer exhibits a long range hexatic order ($\psi_6 > 0.6$, see Table 1). The tilt is in the direction of one of the verteces of the hexagon formed by nearest neighbours, indicating that the phase is Sm_J. This tilted structure persists down to the lowest temperature studied, with an angle $\langle\alpha\rangle$ essentially constant in the range 16°- 18° as reported in Table 1. Also in this case, $\langle P_1^x\rangle_{tot}$ is zero, while $\langle P_1^x\rangle_{\mathcal{L}}$, for the separated odd and even layers, are definitely quite large, even if their absolute values are smaller than for the first case (Table 1). In fact, the layers are only partially polarized showing domains (see Fig. 8) with different dipoles orientations and this wider variety of orientations is reflected also in the reduced phase biaxiality and in the behaviour of the second rank orientational correlation S_{22}^{220}.

Even in this case of tilted phases no detected evidence of not averall chirality as measured by S_{00}^{221} was detected (Fig. 8).

4 Conclusions

We have shown by MC computer simulations of dipolar three site GB molecules that a small change in the point dipoles locations leads to important changes in phase behaviour and may induce nematic and tilted smectic phases for a system of bent–shaped molecules.

At low temperatures these banana–shaped molecules with one central transversal dipole form an untilted smectic phase, with large biaxiality, while no nematic phase is observed. Each layer is locally polarized, but adjacent layers are arranged in an antiferroelectric fashion and the overall sample is not polarized.

Two point dipoles placed at the centres of the lateral sites induce a softening of the disorder–order transition with the appearance of a nematic phase (see Fig. 2),

which is absent in the previous case as in the dipole–less system. The structure of the smectic phase is similar to that observed for the central dipole system.
Moving dipoles towards the terminal positions of bent particles arms has the effect of broadening the nematic phase. At low temperatures tilted smectic layers are formed with average tilt angle in the range of $16° - 18°$. Layers show domains, with size on the order of a few molecular breadths, with different dipoles orientations and this organization reflects in the decrease of phase biaxiality.
Even in the case of tilted layers we did not see a measurable evidence of chirality in this system of rigid achiral polar bent mesogens.

Acknowledgements

We wish to thank University of Bologna, MIUR (PRIN "Cristalli Liquidi", FIRB RBNE01P4JF), and INSTM for financial support.

References

[1] T. Niori, T. Sekine, J. Watanabe, T. Furukawa and H. Takezoe, J. Mater. Chem. **6**, 1231 (1996).

[2] G. Pelzl, S. Diele and W. Weissflog, Adv. Mat. **11**, 707 (1999).

[3] D. Link, G. Natale, R. Shao, J. E. Maclennan, N. A. Clark, E. Körblova and D. M. Walba, Science **278**, 1924 (1997).

[4] B. R. Acharya, A. Primak, T. J. Dingemans, E. T. Samulski and S. Kumar, Pramana-J. Phys. **61**, 231 (2003).

[5] L. Madsen, T. Dingemans, M. Nakata and E. Samulski, Phys. Rev. Lett. **92**, 145505.1 (2004).

[6] D. M. Walba *et al.*, Science **288**, 2181 (2000).

[7] D. Earl, M. Osipov, H. Takezoe, Y. T. M.R. and Wilson, Phys. Rev. E **71**, 021706 (2005).

[8] G. Heppke and D. Moro, Science **279**, 1872 (1998).

[9] J. Thisayukta, H. Niwano, H. Takezoe and J. Watanabe, J. Am. Chem. Soc. **124**, 3354 (2002).

[10] H. Kurosu, M. Kawasaki, M. Hirose, M. Yamada, S. Kang, J. Thisayukta, M. Sonme, H. Takezoe and J. Watanabe, J. Phys. Chem. A **108**, 4674 (2004).

[11] G. Pelzl, A. Eremin, S. Diele, H. Kresse and W. Weissflog, J. Mater. Chem. **12**, 2591 (2002).

[12] R. Berardi, M. Ricci and C. Zannoni, ChemPhysChem **2**, 443 (2001).

[13] C. Zannoni, J. Mater. Chem. **11**, 2637 (2001).

[14] P. J. Camp, M. P. Allen and A. J. Masters, J. Chem. Phys. **111**, 9871 (1999).

[15] Y. Lansac, P. K. Maiti, N. A. Clark and M. A. Glaser, Phys. Rev. E **67**, 011703 (2003).

[16] P. K. Maiti, Y. L. M. A. Glaser and N. A. Clark, Phys. Rev. Lett. **88**, 065504 (2002).

[17] J. L. Xu, R. Selinger, J. V. Selinger and R. Shashidhar, J. Chem. Phys. **115**, 4333 (2001).

[18] A. Dewar and P. J. Camp, Phys. Rev. E **70**, 011704 (2004).

[19] S. J. Johnston, R. J. Low and M. P. Neal, Phys. Rev. E **65**, 051706 (2002).

[20] S. J. Johnston, R. J. Low and M. P. Neal, Phys. Rev. E **66**, 061702 (2002).

[21] R. Memmer, Liq. Cryst. **29**, 483 (2002).

[22] T. Miyazaki and M. Yamashita, Ferroelectrics **276**, 147 (2002).

[23] G. R. Luckhurst, Angew. Chem. Int. Ed. Engl. **44**, 2834 (2005).

[24] R. Berardi, S. Orlandi and C. Zannoni, Chem. Phys. Lett. **261**, 357 (1996).

[25] R. Berardi, S. Orlandi and C. Zannoni, Phys. Rev. E **67**, 041708.1 (2003).

[26] K. Satoh, S. Mita and S. Kondo, Chem. Phys. Lett. **255**, 99 (1996).

[27] A. G. Vanakaras and D. J. Photinos, Molec. Cryst. Liq. Cryst. **395**, 213 (2003).

[28] J. G. Gay and B. J. Berne, J. Chem. Phys. **74**, 3316 (1981).

[29] J. A. Barker and R. O. Watts, Molec. Phys. **26**, 789 (1973).

[30] A. Gil-Vilegas, S. McGrother and G. Jackson, Molec. Phys. **92**, 723 (1997).

[31] M. Houssa, A. Oualid and L. Rull, Molec. Phys. **94**, 439 (1998).

[32] R. Berardi, S. Orlandi and C. Zannoni, Int. J. Mod. Phys. C **10**, 477 (1999).

[33] S. Yashonath and C. N. R. Rao, Molec. Phys. **54**, 245 (1985).

[34] G. Luckhurst and K. Satoh, Molec. Cryst. Liq. Cryst. **394**, 153 (2003).

[35] M. Parrinello and A. Rahaman, Phys. Rev. Lett. **45**, 1196 (1980).

[36] D. Frenkel and B. Smit, *Understanding Molecular Simulation: from Algorithms to Applications* (Academic Press, San Diego, 1996).

[37] F. Biscarini, C. Chiccoli, P. Pasini, F. Semeria and C. Zannoni, Phys. Rev. Lett. **75**, 1803 (1995).

[38] A. Stone, Molec. Phys. **36**, 241 (1978).

[39] R. Berardi and C. Zannoni, J. Chem. Phys. **113**, 5971 (2000).

[40] R. Berardi, M. Cecchini and C. Zannoni, J. Chem. Phys. **119**, 9933 (2003).

[41] A. Jaster, Phys. Rev. E **59**, 2594 (1999).

[42] P. Collings and M. Hird, *Introduction to Liquid Crystals* (Taylor and Francis, London, 1997).

n_{dip}	T^*	$\langle R_{22}^2 \rangle$	$\langle P_1^x \rangle_{tot}$	$\lvert\langle P_1^x \rangle_{\mathcal{L}}\rvert$	$\langle \alpha \rangle$	$\langle \psi_6 \rangle$	Phase
1 (central)	3.4	0.40	-	0.95	-	0.70	Sm_B
	3.6	0.40	-	0.95	-	0.69	Sm_B
	3.7	0.39	-	0.94	-	0.69	Sm_B
	3.8	0.38	-	0.93	-	0.68	Sm_B
	3.9	0.39	-	0.94	-	0.64	Sm_B
	4.0	0.37	-	0.91	-	0.56	Sm_B
2 (lateral)	2.8	0.35	-	0.93	-	0.66	Sm_B
	3.0	0.34	-	0.93	-	0.65	Sm_B
	3.2	0.34	-	0.92	-	0.64	Sm_B
	3.3	0.33	-	0.89	-	0.63	Sm_B
	3.4	0.32	-	0.85	-	0.51	Sm_A
	3.5	0.30	-	0.80	-	0.48	Sm_A
2 (terminal)	2.9	0.16	-	0.53	16°	0.74	Sm_J
	3.0	0.16	-	0.50	17°	0.73	Sm_J
	3.1	0.15	-	0.50	18°	0.72	Sm_J
	3.2	0.11	-	0.53	18°	0.71	Sm_J
	3.3	0.11	-	0.52	18°	0.69	Sm_J

Table 1: Results for biaxial $\langle R_{22}^2 \rangle$ and polar order parameters $\langle P_1^x \rangle$ (global) and $\lvert\langle P_1^x \rangle_{\mathcal{L}}\rvert$ (per layer), tilt angle $\langle \alpha \rangle$, hexatic order parameter $\langle \psi_6 \rangle$ and type of smectic phase for the three systems studied at different temperatures T^*.

List of Figures

Figure 4: One central dipole.(**a**) Lateral (**Y**) view of an exploded view of a smectic B snapshot at $T^* = 3.8, P^* = 10$ as obtained from NPT MC simulations. The colour code indicates the orientation of the molecular **x** axis. (**b**) A first (**b**) and a second (**c**) rank pair correlation.(Color online)

Figure 5: Two lateral dipoles.(**a**) Lateral (**Y**) view of a smectic B snapshot at $T^* = 2.8, P^* = 10$ as obtained from NPT MC simulations. The colour code indicates the orientation of the molecular **z** axis. (**b**) Radial correlation function $g(r)$; (**c**) density along the director $g(z)$. (Color online)

Figure 6: Two lateral dipoles.(**a**) Lateral (**Y**) view of an exploded view of a smectic B snapshot at $T^* = 2.8, P^* = 10$ as obtained from NPT MC simulations. The colour code indicates the orientation of the molecular **x** axis. A first (**b**) and a second (**c**) rank pair correlation. (Color online)

Figure 7: Two terminal dipoles.(**a**) lateral (**Y**) view of a smectic B snapshot at $T^* = 3.2, P^* = 10$ as obtained from NPT MC simulations. The colour code indicates the orientation of the molecular **z** axis. (**b**) Radial correlation function $g(r)$; (**c**) density along the director $g(z)$. (Color online)

Figure 8: Two terminal dipoles. (**a**) Lateral (**Y**) view of an exploded view of a smectic J snapshot at $T^* = 3.2, P^* = 10$ as obtained from NPT MC simulations. The colour code indicates the orientation of the molecular **x** axis. A first (**b**) and a second (**c**) rank pair correlation, and (**d**) a chiral pair invariant. (Color online)

Figure 1

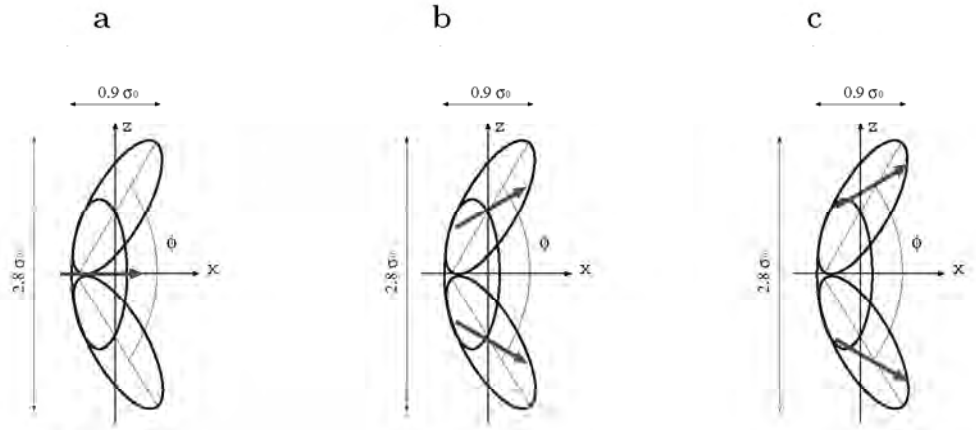

Figure 2

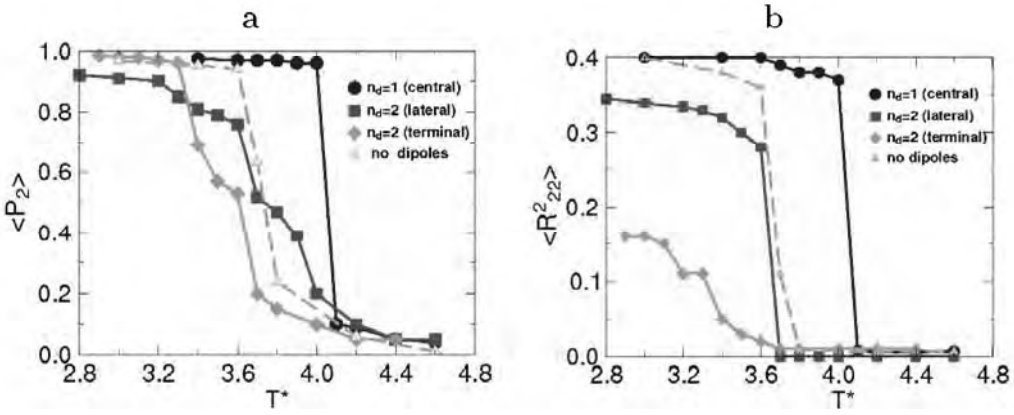

Figure 3

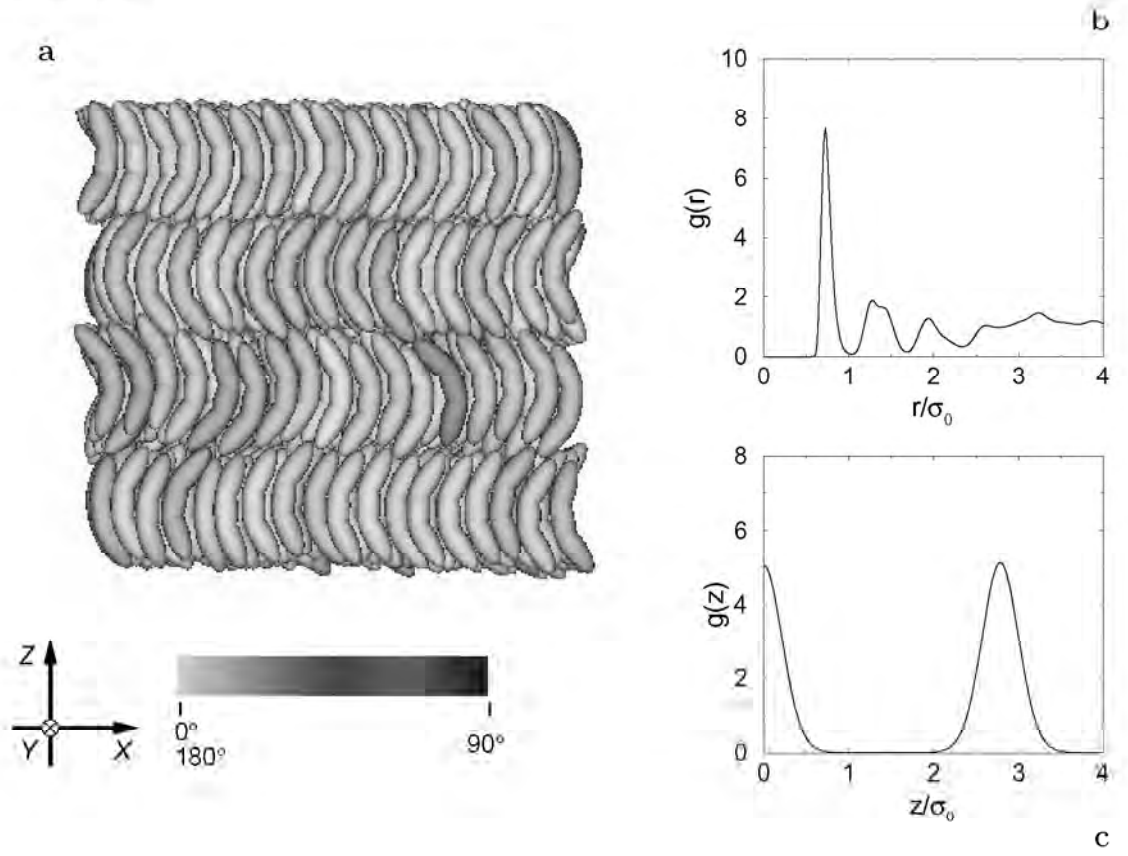

Figure 4

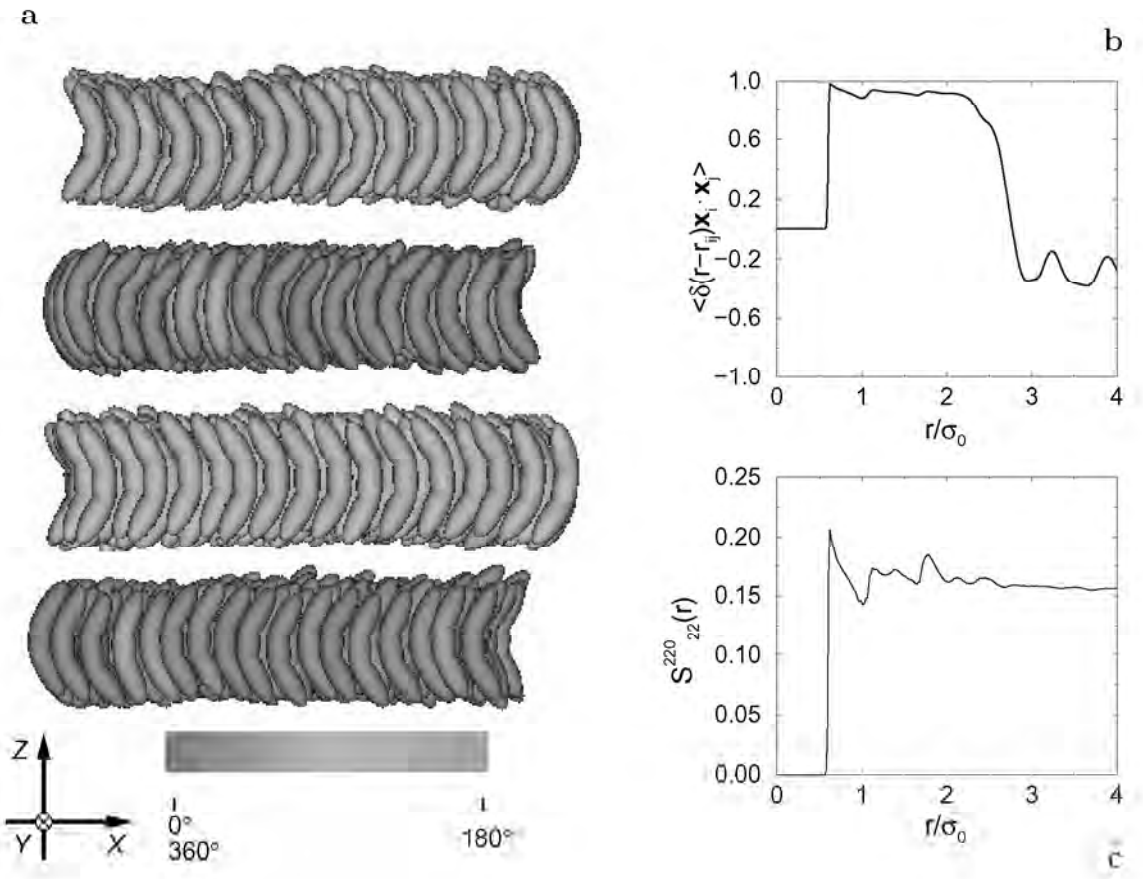
a
b
Z
Y
X
0°
360°
180°
1.0
0.6
0.2
−0.2
−0.6
−1.0
0
1
2
3
4
r/σ0
<δ̃(r−rij)xi · xj>
0.25
0.20
0.15
0.10
0.05
0.00
S220 22(r)
r/σ0
c

Figure 5

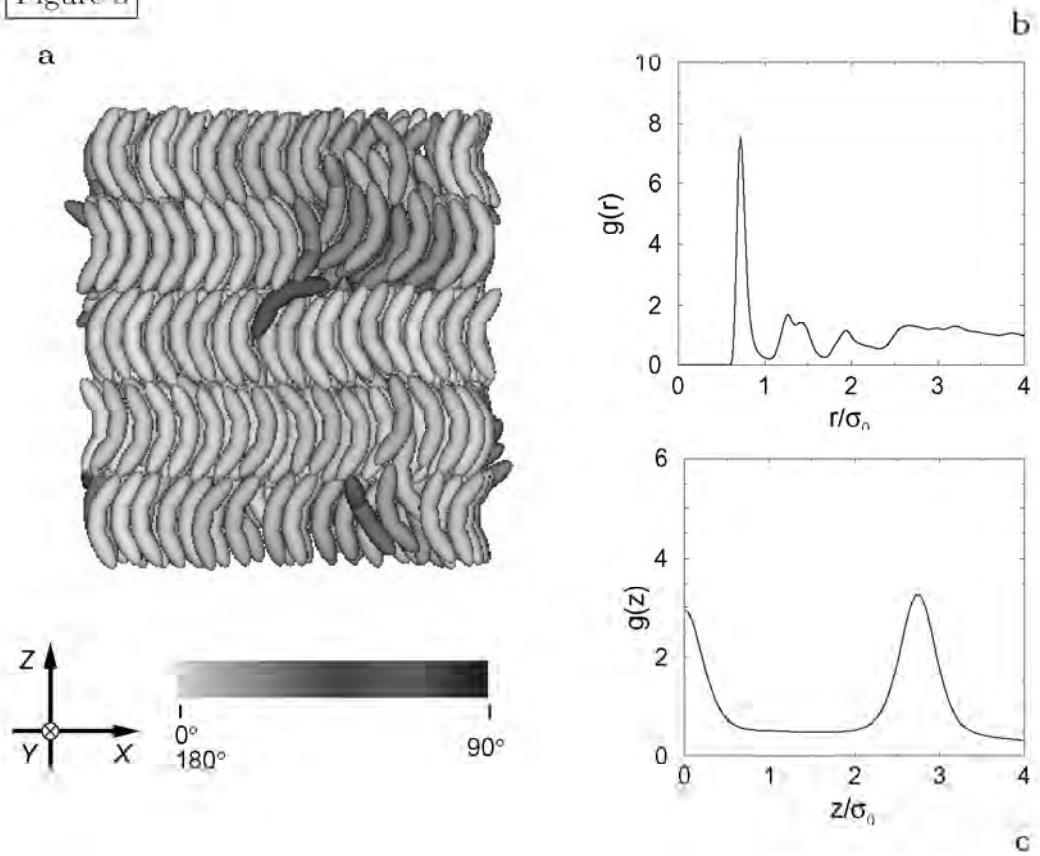

Figure 6

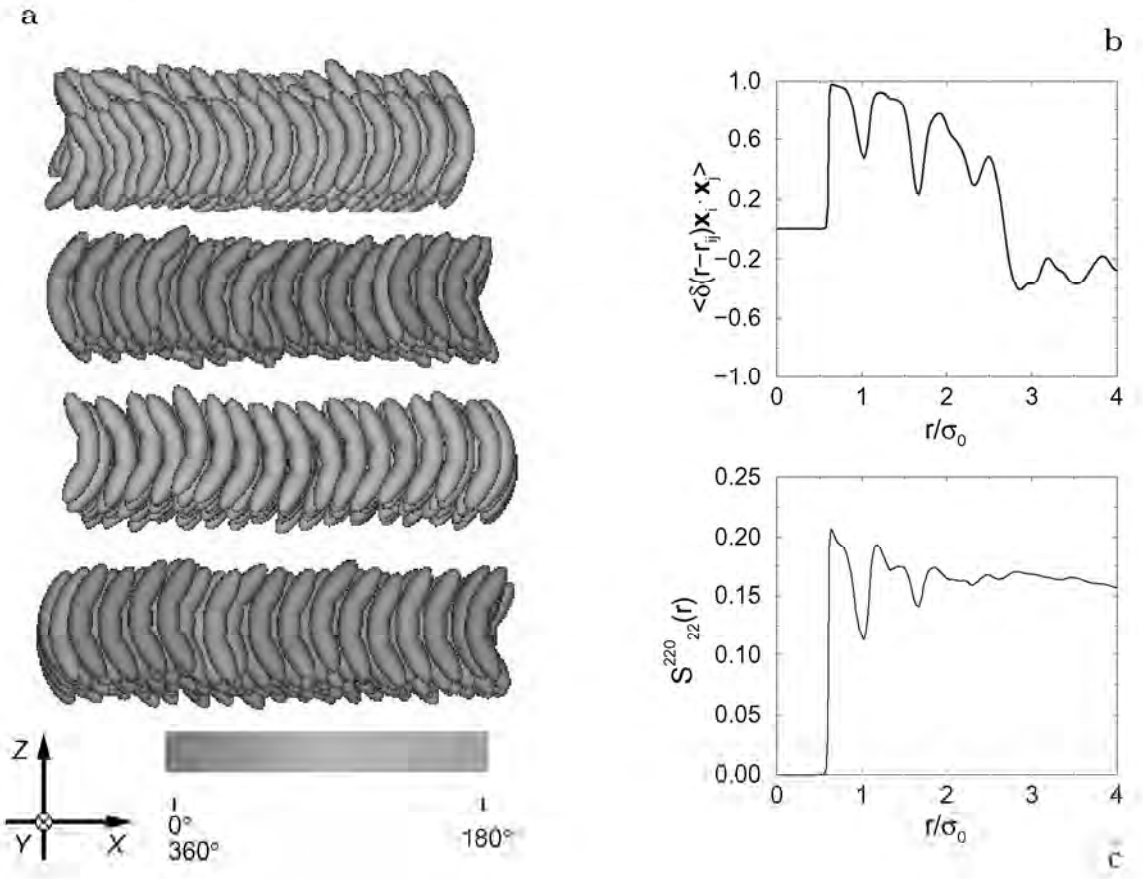
a
b
Z
Y
X
0°
360°
180°
1.0
0.6
0.2
−0.2
−0.6
−1.0
0
1
2
3
4
r/σ0
<δ̃(r−rij)xi · xj>
0.25
0.20
0.15
0.10
0.05
0.00
S220 22(r)
r/σ0
c

Figure 7

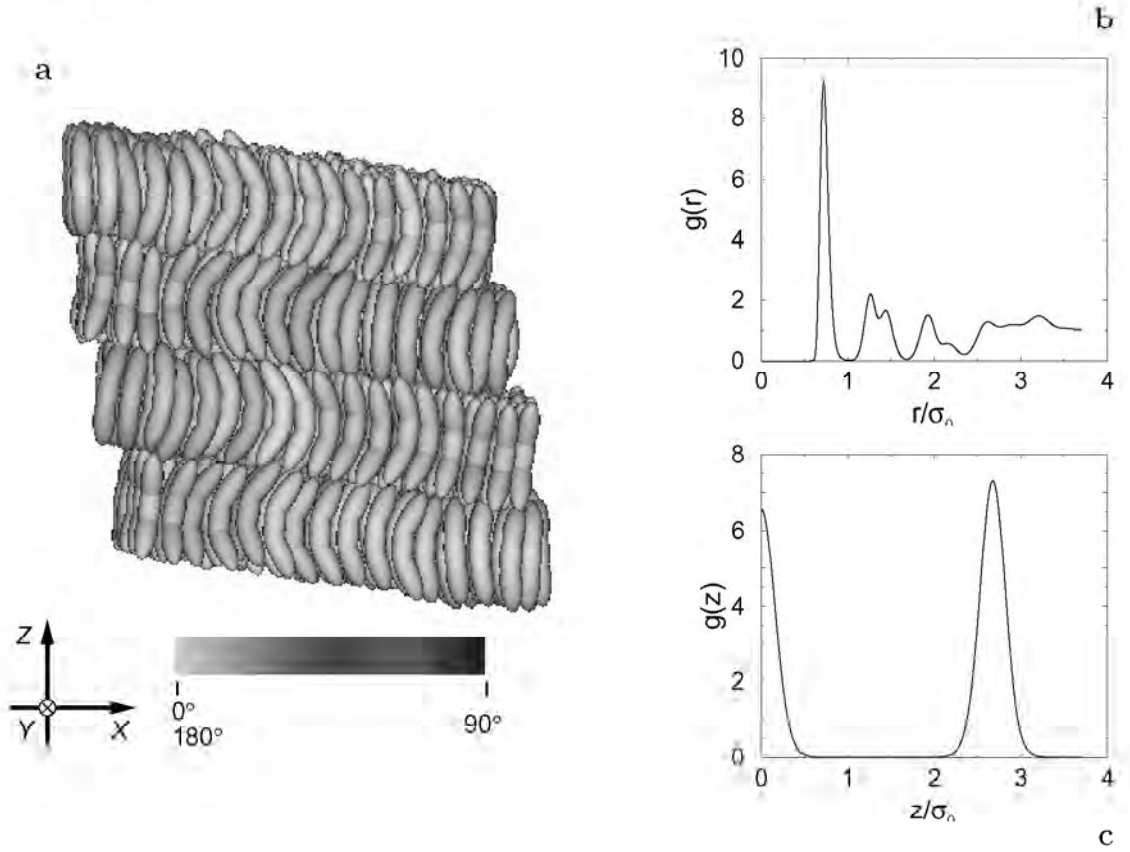

Figure 8

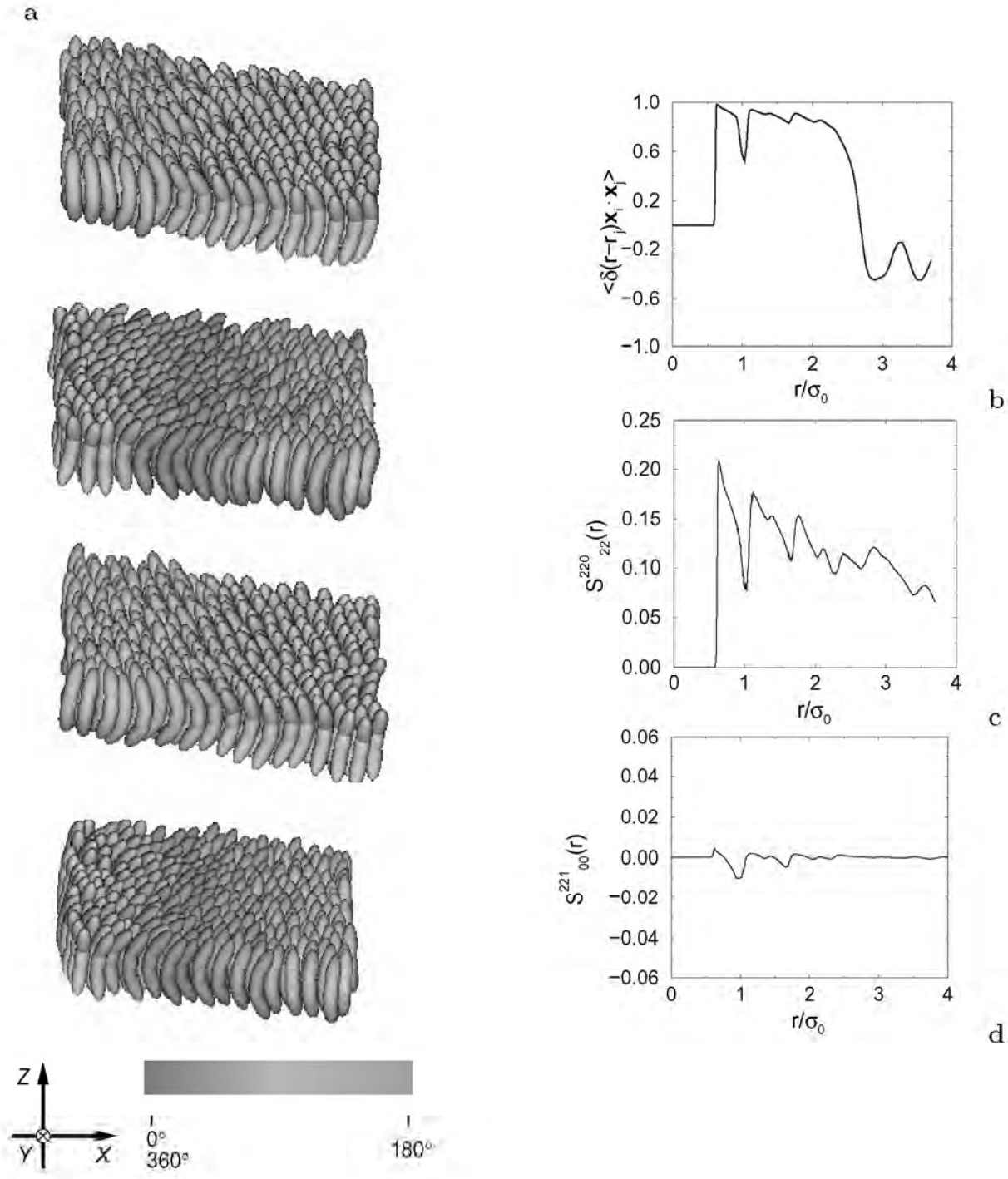
a
Z
Y
X
0°
360°
180°
1.0
0.6
0.2
−0.2
−0.6
−1.0
<δ(r−r_j)x_i · x_j>
0
1
2
3
4
r/σ_0
b
0.25
0.20
0.15
0.10
0.05
0.00
S^220_22(r)
r/σ_0
c
0.06
0.04
0.02
0.00
−0.02
−0.04
−0.06
S^221_00(r)
r/σ_0
d